Applied Thermal Engineering 246 (2024) 122923

Contents lists available at ScienceDirect

Applied Thermal Engineering

journal homepage: www.elsevier.com/locate/apthermeng

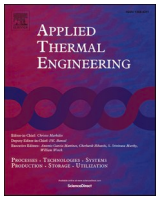

Research Paper

Enhancement of the Power-to-Heat Energy Conversion Process of a Thermal Energy Storage Cycle through the use of a Thermoelectric Heat Pump

I. Erro [a], P. Aranguren [a,*], F.J. Sorbet [b], I. Bonilla-Campos [c], D. Astrain [a]

[a] Institute of Smart Cities, Public University of Navarre, Pamplona, Spain
[b] Solar Energy Technologies & Storage Department, CENER (National Renewable Energy Centre of Spain), Sarriguren, Spain
[c] AIN Asociación de la Industria Navarra, Cordovilla, Navarra, Spain

ARTICLE INFO

Keywords:
COP
Energy Management
Power-to-Heat
Thermal Energy Storage
Thermoelectric Heat Pump

ABSTRACT

The principal strategy for achieving a neutral climate entails enhancing the share of renewable energies in the energy mix, in conjunction with promoting innovation in efficient technologies. Thermal energy storage systems have the potential to efficiently handle the intermittent nature of renewable energy sources. Furthermore, these systems can effectively handle shifts in both heat and electrical demand. Thus, efficient power-to-heat technologies are needed to boost thermal energy storage. This manuscript explores the potential of utilising a thermoelectric heat pump system in conjunction with electric resistances for charging a thermal energy storage. In order to achieve elevated temperatures, the thermoelectric system integrates thermoelectric heat pump blocks in a two-stage configuration. Air has been employed as a heat transfer medium for sensible heat storage. Higher airflow rates improve the performance of thermoelectric heat pump system. Moreover, its impact on the optimal voltage supply of the thermoelectric system is observed when it is combined with an electric resistance to achieve elevated temperatures. In comparison to the basic charging process that solely relies on the electric resistance of a thermal energy storage at 120 °C, a significant 30 % increase in power-to-heat energy conversion has been achieved by including the thermoelectric heat pump system. In fact, it efficiently elevates the temperature from the initial ambient temperature of 25 °C to a remarkable 113.1 °C, achieving a coefficient of performance of 1.35 with an airflow rate of 23 m^3/h. Therefore, the use of this technology to enhance a complete process of storing excess renewable energy in the form of heat for subsequent use in both heat and electricity through a combined heat and power cycle is demonstrated.

1. Introduction

The imperative to address climate change has resulted in an increased integration of renewable energies (REs) into the energy mix [1]. This integration aligns with the global Sustainable Development Goals (SDGs), particularly with the 7th SDG, which highlights the pivotal role of clean and sustainable energy practices in achieving a more resilient and environmentally responsible future [2]. Within the European Union (EU), the share of RE sources in its gross final energy consumption reached 21.8 % in 2021, representing a 3.8 points increase compared to 2016 [3]. Moreover, the share of renewable energy sources in Europe is projected to grow, with a target of 42.5 % by 2030 [4]. Nonetheless, the intermittent nature of RE sources that is attributed to climate conditions leads to variations in electricity generation and predictable alterations in the energy generation curve [5]. Therefore, energy storage (ES) systems are essential. In particular, thermal energy storage (TES) presents an attractive option for energy management [6]. TES systems store energy in the form of heat, providing flexibility in aligning the supply and demand of electricity [7], as well as heating and cooling generation [8]. TES application enhance both centralised and decentralised energy systems [9], promoting heat and electricity sector coupling [10].

TES can be classified into three distinct types: sensible heat storage (SHS), latent heat storage (LHS), and thermochemical heat storage (TCHS). SHS is based on the temperature increase of a liquid or solid medium. Because of its simplicity and affordability, the SHS is the most utilised TES technology, offering storage efficiencies between 50 and 90 % [11]. Latent heat storage (LHS) uses a phase-change material to store energy as latent heat. LHS presents a higher energy density, with an efficiency ranging from 75 to 90 % [11]. Finally, TCHS systems store and release heat by a reversible endothermic/exothermic reaction process.

* Corresponding author.
E-mail address: patricia.arangureng@unavarra.es (P. Aranguren).

https://doi.org/10.1016/j.applthermaleng.2024.122923
Received 13 October 2023; Received in revised form 5 March 2024; Accepted 10 March 2024
Available online 11 March 2024
1359-4311/© 2024 The Authors. Published by Elsevier Ltd. This is an open access article under the CC BY-NC license (http://creativecommons.org/licenses/by-nc/4.0/).

Nomenclature

A	Airflow duct transversal section, m^2
I_j	Current supply of j thermoelectric block, A
$\dot{m}_{air}$	Air mass flow, kg/s
P_{shaft}	Expander shaft power, W
P_h	Useful heat power, W
$\dot{Q}_c$	Absorbed heat, W
$\dot{Q}_h$	Generated heat, W
$\dot{v}_{air}$	Airflow rate, m^3/h
ρ_{air}	Airflow density, kg/m^3
c_{pair}	Airflow heating capacity, J/kgK
η	Efficiency
R_{cHX}	Thermal Resistance of cold-side heat exchanter, K/W
T	Airflow Temperature, °C
T_j	Airflow outlet temperature of j thermoelectric block, °C
$T_{c,j}$	TEHP cold-side Temperature of j thermoelectric block, °C
T_{in}	Inlet Temperature to the cycle, °C
T_s	Duct superficial Temperature, °C
T_i	Isolation superficial Temperature, °C
V_j	Voltage supply of j thermoelectric block, V
$\dot{W}_e$	Power supply, W

Subscripts

in, TES	Inlet of the thermal energy storage
$out, TEHP$	Outlet of the thermoelectric heat pump system
out, TES	Outlet of the thermal energy storage

Acronyms

CHP	Combined Heat and Power
COP	Coefficient of Performance
EU	European Union
ES	Energy Storage
HP	Heat Pump
ORC	Organic Rankine Cycle
PtH	Power-to-Heat
OTEHP	One-stage Thermoelectric Heat Pump
PtHtP	Power-to-Heat-to-Power
PtHtCHP	Power-to-Heat-to-Combined Heat and Power
R_e	Electric Resistance
RE	Renewable energy
TEHP	Thermoelectric Heat Pump
TEM	Thermoelectric module
TTEHP	Two-stage Thermoelectric Heat Pump
VCHP	Vapour compression Heat Pump

TCHS present the greatest efficiencies between 75 and 100 % [11]. In order to enhance the storage efficiencies, different storage mediums [12–14] and layouts [15–19] have been widely studied. When renewable electricity is used to charge the thermal storage, it is necessary to include the power-to-heat (PtH) energy conversion efficiency in the calculation of the overall storage efficiency. As well as it is necessary to consider the efficiency of the heat-to-power energy conversion when reconverting stored thermal energy into electricity [20].

Extensive studies have been conducted on the process of converting thermal energy into electrical energy in thermal power plants, which can also be employed for thermal energy discharge in thermal energy storage [21]. Steam Rankine cycles are widely employed as a heat-to-power technology, particularly with high-grade heat sources. The efficiencies of present-day subcritical power plants, which incorporate reheating at temperatures of around 540 °C and a pressure of 17 MPa, typically fall within the range of 33 to 39 %. Additionally, operating at pressures close to 25 MPa and temperatures spanning from 540 to 560 °C, supercritical cycles are capable of achieving thermal efficiencies of 43 to 45 %. Moreover, advanced ultra-supercritical cycles demonstrate efficiencies of approximately 50 % while operating at 35 MPa and 700 °C [22]. At lower heat – grade sources other cycles such as the organic Rankine cycles (ORCs) are more suited [23]. However, the efficiencies of these cycles are generally low, which are expected to be around 5–23 % when the heat source temperature is between 100 and 200 °C [24], depending on operation conditions, working fluid and cycle configuration [25]. As a result, there is a significant interest in the utilisation of these cycles for combined heat and power (CHP) systems in order to maximise energy efficiency [26].

In the context of the PtH process, there is presently a great deal of interest in identifying efficient technologies in order to store renewable energy as heat. In particular, the most used PtH technology has been the electric resistance (R_e). An electric resistance converts electricity into heat by Joule effect when the electric current passes through it. This energy conversion technology stands out due to its simplicity and easy control. Thus, its application has started to study for energy management. Eggers *et al.* [27] used electric resistances to store the surplus of renewable energy in a SHS at 480 °C to then reconvert it with a Steam Rankine Cycle into electricity. Labairu *et al.* [28] incorporated an electric resistance in a concentrated solar power electric generation plant to store surplus of RE from a photovoltaic solar plant, maximising the energy efficiency. Hu *et al* [29] presented a techno-economic study that utilises electric resistances to charge a TES for power-to-heat conversion. This strategy effectively manages the variations in renewable energy and supplies a CHP system reaching thermal efficiencies of 99.19 %.

One effective measure to enhance performance in these TES applications is by improving the power-to-heat energy conversion process. The performance assessment of PtH technologies is based on the coefficient of performance (*COP*), which quantifies the ratio of generated heat to electric power consumption. The coefficient of performance for electric resistances is limited to the unit [30]. As a result, the use of heat pumps (HP) in PtH processes has garnered increased attention in recent years due to their capacity to achieve *COP* values that surpass the unit. The heat dissipated from the heat pump to the hot source is equal to the sum of the heat absorbed from the cold source and the electric power consumed. Ongoing research is focused on the development of high-temperature heat pumps that can generate heat within the temperature range of 100–200 °C. This capability allows for promising integration with various processes, including thermal energy storage, low-grade waste heat recovery, organic Rankine cycle, cogeneration, and poly-generation [31]. Vapour compression heat pumps (VCHPs) are widely regarded as the most popular HP technology. They are comprised of an evaporator, a condenser, a compressor, and refrigerant as the working fluid. However, the critical properties of refrigerants limit the operating temperature range, which leads to the use of more complex configurations in order to achieve high temperatures with relative high *COP* values. [32–35].

Therefore, a thermoelectric heat pump (TEHP) serves as an alternative to VCHP technology. It consists of thermoelectric modules (TEMs) that are commonly formed by two ceramic plates and N number of thermocouples formed by n- and p-semiconductor junctions, connected thermally in parallel and electrically in series. When a current is supplied, heat is pumped from the cold sink to the hot sink by Peltier effect [36]. Thermoelectric technology boasts a range of advantages, including the elimination of refrigerants, ease of control, absence of moving parts, modular design, reliability, autonomy from auxiliary components, and installation flexibility. All these advantages have increased the interest in using this technology for heating applications in recent years. Diaz de Garayo *et al.* [37] studied different the combination of a TEHP with a

heat recovery unit for heating different airflows. According to their findings, there was a maximum temperature increase of 50 °C in the air, resulting in *COP* values ranging from 1.5 to 4. Hou *et al.* [38] stated that the use of air recirculation makes the temperature between the two sides of the TEHP smaller, which is beneficial for the *COP* of the TEHP. Specifically, the authors achieved a *COP* value of 3.7 with air recirculation and a temperature rise of 4.5 °C in the heated airflow with a velocity of 1 m/s. Nevertheless, to reach higher temperatures with efficient thermoelectric systems more than two-stage thermoelectric heat pumps are recommended. Nami *et al.* [39] computationally demonstrated that using a two-stage configuration results in better performance than a TEHP system for heating, being able to operate at higher temperature differences with higher *COP* values. Thus, some computational studies are found in order to optimise two-stage configurations for heating applications. Chen. *et al.* [40] provided a demonstration of the existence of an optimal relationship between the number of thermocouples between stages, which affects both the *COP* and the heating capacity. Arora *et al.* [41] demonstrated that a parallel connection of an optimised pyramidal two-stage thermoelectric heat pump obtains higher *COP* values when comparing with series connection between stages. L.G. Chen *et al.* [42] stated the crucial role of the external heat exchangers in determining the working temperatures and thereby impacting the performance. In light of the limited availability of experimental results, earlier research efforts were dedicated to the design and experimentally study of a pyramidal two-stage thermoelectric heat pump module, incorporating an optimised intermediate heat exchanger [43]. Furthermore, a sensitivity study was conducted to evaluate its performance in comparison to a one-stage thermoelectric heat pump and a square two-stage thermoelectric heat pump without an intermediate heat exchanger [44]. It was shown that a two-stage configuration is required when dealing with high temperature differences, whereas the one-stage configuration is the most suitable option for low temperature differences.

Based on the literature, a novel thermoelectric heat pump system has been developed for achieving high temperatures. In particular, for the first time, the potential of thermoelectricity as a power to heat technology has been analysed. Thus, a real prototype of TES based on electrical resistance has been built, where a thermoelectric heat pump system has been incorporated into the power-to-heat process. Therefore, this manuscript is arranged as follows: section 2 outlines the development of the experimental setup, the utilisation of data acquisition equipment, and the experimental methodology. Following that, a thorough examination of the performance of the developed thermoelectric heat pump system is conducted in Section 3. This involves varying the airflow rate and voltage supply. Section 4 assesses the integration of the thermoelectric heat pump system with the electric resistance in the PtH process, considering varying storage temperatures, voltage supply, and airflow rates. In Section 5, the assessment of the airflow rate and storage temperature during the TES charging process is discussed. Additionally, Section 6 explores the potential integration of the prototype into a power-to-heat-to-power system, which examines not only electricity generation but also combined heat and power production.

2. Experimental system

2.1. Thermal energy storage cycle

The following section details with the design of the thermal energy storage cycle used for experimentation. Fig. 1 illustrates the TES cycle that relies on an open cycle with air as a heat transfer fluid. Utilising air as a heat transfer fluid offers numerous benefits, including its abundance and cost-effectiveness, non-toxicity, versatility in temperature ranges, decreased corrosion, and scalability. In particular, the used TES cycle includes four main components: a fan (1), a thermoelectric heat pump system (2), an electric resistance (3), and thermal energy storage (4).

The fan CMP-620–2 T/R from SODECA is positioned at the air inlet of the cycle, controlling the airflow rate through a variable speed drive control. Then, the TEHP system is installed for heating the airflow, which configuration is explained in the subsequent section. Particularly, the TEHP system aims to attain the highest air heating with the best *COP* possible. Subsequently, an electric resistance is installed to complement the TEHP system. The maximum air heating capacity of the used electric resistance is 1666 W, with controlled heat generation to achieve the desired inlet storage temperature. Finally, the thermal energy storage is located.

Additionally, four sectioning valves (V1, V2, V3 and V4) are collocated during the cycle to enable two different operating modes: preheat mode and charge mode. The preheat mode (V1, V3 = ON, V2, V4 = OFF)

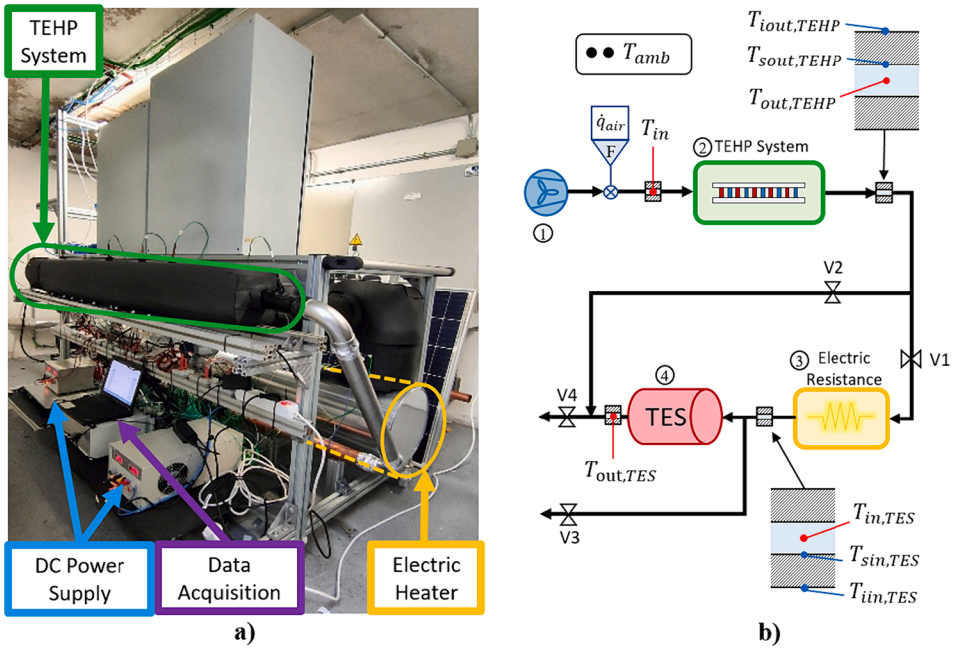

Fig. 1. a) tes facility b) schematic of the tes system.

is used to stabilise the cycle temperature before starting a test. Its purpose is to ensure that all system elements reach the necessary temperatures during testing, thus avoiding thermal inertia. The charge mode (V1, V4 = ON, V2, V3 = OFF) is employed during a test wherein the heated airflow traverses the TES by closing valve 3 and opening valve 4. The sequential utilisation of the preheat mode followed by the charge mode guarantees that the heat gained by the air is exclusively utilised for the purpose of charging the storage system, rather than heating the pipes of the system. In addition, the experimental system has undergone meticulous insulation with rock wool to eliminate any heat loss to the environment while in operation.

2.2. Thermoelectric heat pump system

The constructed thermoelectric heat pump system consists of six TEHP blocks arranged in series in a duct to heat up an airflow, as it is shown in Fig. 2. In this way, the heated air flow is considered to be the hot source of the TEHP system and the ambient air is considered as the cold source. The airflow heats up as it passes through the thermoelectric blocks, increasing the temperature difference between the hot and cold source of the TEHP. Therefore, for the first three blocks, one-stage thermoelectric heat pump (OTEHP) configuration is used as it gives the best performance for small temperature differences between heat sources [44]. Each OTEHP block is based on a unique TEM (Marlow RC12-6-01LS [45]) with one heat exchanger on each side. The subsequent three TEHP blocks comprise two-stage thermoelectric heat pumps (TTEHP). TTEHP configuration provides better performance than a one-stage configuration when the temperature differential between the hot and cold sources is high [39]. Specifically, a pyramidal TTEHP configuration was used, with one TEM (Marlow RC12-6-01LS [45]) in the first stage and two TEMs (Marlow TG12-6-01LS [46]) in the second stage, thermally connected by an intermediate phase-change heat exchanger. The design of this intermediate heat exchanger utilises a highly efficient system comprised four heat pipe tubes with water as working fluid [43]. The transfer of heat from the first stage to the second stage occurs through these tubes by means of phase change of water. Both thermoelectric configurations use the same cold and hot side heat exchangers. For the cold side, a finned heat exchanger has been used, based on an aluminium finned dissipator with a base of 73 x 73 mm^2 and a height of 14.5 mm, and 15 fins with height, spacing and thicknesses of 38.5; 3.4 and 1.6 mm respectively. In addition, an axial fan was placed opposite the fins to control the ambient airflow. For the hot side of each thermoelectric module, a commercial heat pipe, JONSBO CR-1400 ARGB, was used to help dissipating the heat to the airflow.

2.3. Data acquisition and measurement equipment

The entire prototype is fully monitored by a data acquisition system. Nine immersion (in red), ten contact (in blue) and two ambient (in black) K-type temperature sensors have been installed for temperature measurement, as shown in Figs. 1 and 2. Fig. 1 shows the cycle air inlet temperature (T_{in}); the TEHP system air outlet temperature ($T_{out,TEHP}$) the TES inlet temperature ($T_{in,TES}$) and the TES outlet temperature ($T_{out,TES}$). The above temperature sensors are immersion sensors. In addition, contact temperature sensors are placed on the duct and on the insulation material at the TEHP system outlet ($T_{sout,TEHP}$, $T_{iout,TEHP}$) and at the TES inlet ($T_{sin,TES}$, $T_{iin,TES}$) to determine the end of the preheat mode and to ensure that no heat is lost to the environment. Finally, there are two ambient temperature sensors (T_{amb}). Fig. 2 shows the rest of the temperature sensors, the six airflow outlet temperatures, one immersion sensor per thermoelectric block (T_j) and the six cold-side temperatures ($T_{c,j}$) with contact sensors, where the subscript j indicates the block number. The power consumption was measured independently on each TEHP block using six pairs of ammeters (I_j) and voltmeters (V_j). Finally, the air flow rate was measured using a vortex air flow meter (Fig. 1 (F)) with a measuring range of 6.8—32 m^3/h at 20 °C. The resolution and accuracy of all the measuring equipment is detailed in the Table 1. Labview software is used to process all the measurement data and to control the air flow rate and air inlet temperature to the TES by controlling the fan speed drive and the power consumption of the electric resistances, respectively.

2.4. Experimental methodology

In this work, forty-five different scenarios were experimentally studied, evaluating different airflow rates ($\dot{v}_{air}$), storage temperatures and TEHP system power supply values, as detailed in Table 2. Fig. 3 presents the experimental methodology sequence through a flow chart. At the beginning of each test, the system was preheated to avoid thermal inertia during operation. Once the temperature of the system was established, all tests were carried out with the charging mode selected. The tests were defined as complete when the difference between the inlet and outlet temperatures of the TES was less than 40 °C. Thus, each storage temperature and airflow rate was associated with different test times. Maximum test times of 3, 4.5 and 5.7 h were required when investigating storage temperatures of 120, 160 and 200 °C respectively. During the tests, the TEHP system and the electric resistance operated in steady state, while the TES operated in transient mode. The sampling frequency used was 30 s and the test campaign was also conducted in a controlled ambient temperature of 22 °C.

The performance of the TEHP system is quantified by COP_{TEHP}, which is calculated by Eq.1 [47]. It relates the heat produced $\left(\dot{Q}_{h,TEHP}\right)$ to the

Table 1
Resolution and accuracy of the measurement's sensor used.

Sensor	Type	Resolution	Accuracy
Temperature (°C)	NiCr Type K	0.1	± 0.5
Voltmeter (V)	ZA9900AB4	0.1	± 0.2
Ammeter (A)	ZA9901AB4	0.01	± 0.02
Air flow meter (m^3/h)	OPTISWIRL series 4200	0.1	± 1.5 % of the measure value (10000 < Re < 20000) ± 2.5 % of the measure value Re > 20000)

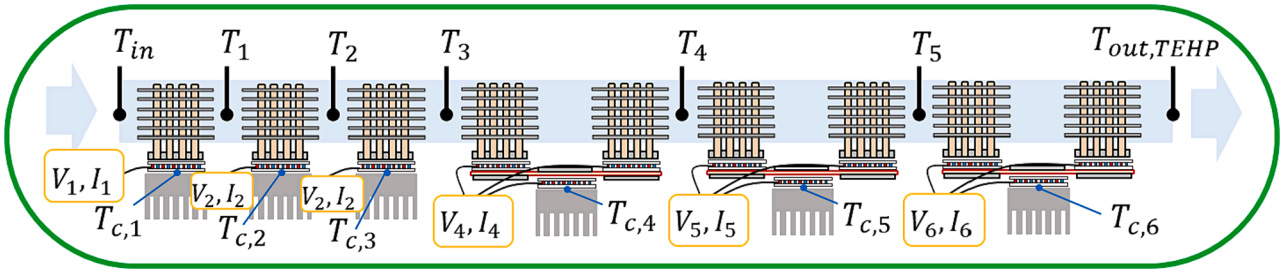

Fig. 2. Schematic of the thermoelectric heat pump system.

Table 2
Experimental tests.

Scenario	Storage inlet temperature ($T_{in,TES}$) [°C]	Airflow rate ($\dot{v}_{air}$) [m³/h]	TEHP voltage (V_j) [V]
1–5	120	13	4, 6, 8, 10, 12
6–10	120	18	4, 6, 8, 10, 12
11–15	120	23	4, 6, 8, 10, 12
16–20	160	13	4, 6, 8, 10, 12
21–25	160	18	4, 6, 8, 10, 12
26–30	160	23	4, 6, 8, 10, 12
31–35	200	13	4, 6, 8, 10, 12
36–40	200	18	4, 6, 8, 10, 12
41–45	200	23	4, 6, 8, 10, 12

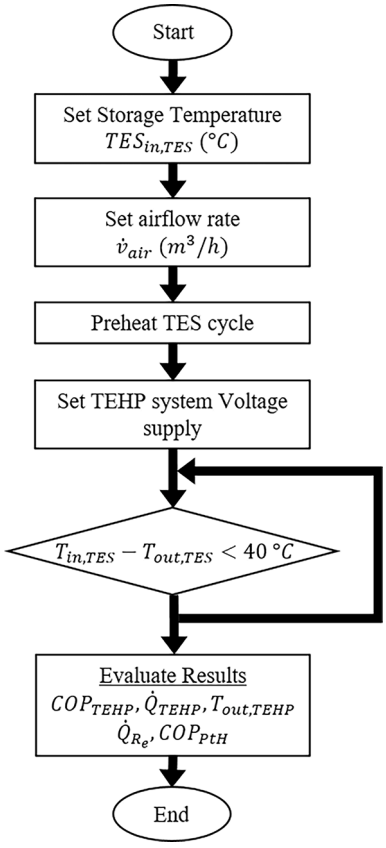

Fig. 3. Flow chart of the experimental methodology.

power consumed $\left(\dot{W}_{e,TEHP}\right)$ by the TEHP system.

$$COP_{TEHP} = \frac{\dot{Q}_{h,TEHP}}{\dot{W}_{e,TEHP}} \quad (1)$$

The power consumed by the TEHP system is obtained by Eq. (2), while $\dot{Q}_{h,TEHP}$ can be calculated by two different methodologies [43]. One method uses the conventional methodology by using Eq. (3) [47], where $\dot{Q}_{h,TEHP}$ is defined by the airflow temperature rise $(T_{out,TEHP} - T_{in})$, the air specific heating capacity (c_{pair}) and the air mass flow $(\dot{m}_{air} = \rho_{air}\dot{v}_{air})$. The second method uses Eq. (4) [43], which describes the heat generated as the sum of the power consumed and the heat absorbed $(\dot{Q}_{c,TEHP})$ by the TEHP from the environment. $\dot{Q}_{c,TEHP}$ is obtained by Eq. (5) [43], which relates the temperature difference between the cold side of each TEHP block and the ambient temperature by the thermal resistance of the cold side heat exchanger (R_{cHX}), which was determined to be 0.333 K/W [43]. Both methods have been used to calculate the generated heat.

The empirical approaches, as demonstrated in Fig. 4, exhibit a discrepancy of less than ± 10 %, thus affirming the reliability of the calculated heat values generated for the thermoelectric heat pump system.

$$\dot{W}_{e,TEHP} = \sum V_j I_j \quad (2)$$

$$\dot{Q}_{h,TEHP} = \dot{m}_{air} c_{pair} (T_{out,TEHP} - T_{in}) \quad (3)$$

$$\dot{Q}_{h,TEHP} = \dot{Q}_{c,TEHP} + \dot{W}_{e,TEHP} \quad (4)$$

$$\dot{Q}_{c,TEHP} = \sum (T_{amb} - T_{c,j})/R_{cHX} \quad (5)$$

For the full system performance analysis, the total $COP_{tot,PtH}$ is calculated by Eq. (6) [47], taking into account the heat produced $\left(\dot{Q}_{h,R_e}\right)$ and the power consumed $\left(\dot{W}_{e,R_e}\right)$ by the electric resistance (R_e). In this case, $\dot{Q}_{h,R_e}$ and $\dot{W}_{e,R_e}$ are considered equal and are calculated by Eq. (7) [47], which depends on the air temperature rise in the electric resistance and the air mass flow.

$$COP_{PtH} = \frac{\dot{Q}_{h,TEHP} + \dot{Q}_{h,R_e}}{\dot{W}_{e,TEHP} + \dot{W}_{e,R_e}} \quad (6)$$

$$\dot{W}_{e,R_e} = \dot{Q}_{h,R_e} = \dot{m}_{air} c_{pair} (T_{in,TES} - T_{out,TEHP}) \quad (7)$$

The uncertainty of the experimental results has been calculated using Eq. (8) [48]. The coefficient 2 corresponds to a confidence interval of the 95 %. b_R is the systematic standard uncertainty that depends on the measurement equipment accuracy detailed in Table 1, and, $s_{\overline{R}}$ stands for the random standard uncertainty for the measurement, representing the inherent variability in the measurement process.

$$U_R = 2\left(b_R^2 + s_{\overline{R}}^2\right)^{1/2} \quad (8)$$

3. Experimental analysis of the thermoelectric heat pump system

The degree of improvement attained in the charging process of a TES depends on the performance of the TEHP system. Therefore, it is essential to understand the behaviour of the installed thermoelectric system. To this end, the behaviour of the thermoelectric heat pump is

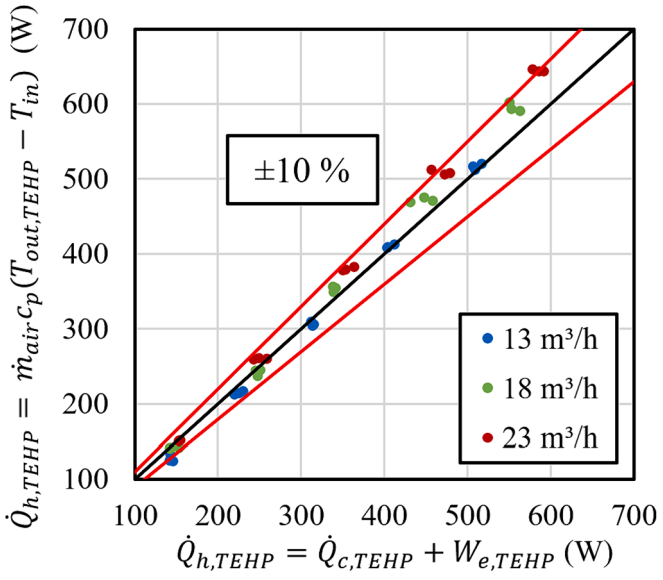

Fig. 4. Correlation of the TEHP heat generation calculated by Eq (3) and Eq (4).

studied under operating conditions where the airflow rate and the power supply have been varied. All tests have been carried out for at least 20 min under stationary conditions with a sampling frequency of 30 s. In addition, the experimental uncertainties calculated by Eq. (8) are included, being less than ± 6.6 % and ± 4.6 % for the COP_{TEHP} and $\dot{Q}_{h,TEHP}$, respectively.

Figs. 5 and 6 show the variation of the COP_{TEHP} as a function of the generated heat and the airflow outlet temperature, respectively, for different airflow rates. In fact, the heat generated and the airflow outlet temperature are directly related to the power supplied. The higher the power supplied, the more heat is generated, so the heat transfer fluid absorbs more heat and increases its final temperature.

As expected, in all the airflows studied, the COP_{TEHP} value decreases with the increase of the heat generated, and therefore with the increase of the airflow temperature. As shown in Fig. 5, the maximum $\dot{Q}_{h,TEHP}$ of 655.5 W is achieved with a COP_{TEHP} value of 1.35 when using the highest airflow rate and reaching 113.1 °C. It also shows how the TEHP system performs better at higher airflow rates for the same heat power output requirement. For instance, to generate 0.5 kW of heat, the COP_{TEHP} values are 1.14, 1.32 and 1.46 at airflows of 13, 18 and 23 m^3/h, respectively. This is because a higher airflow rate reduces the thermal resistance of the hot-side HX and also decreases the temperature rise of the airflow through the TEHP blocks, resulting in lower airflow outlet temperatures. In this case, the latter one is the main reason for the COP_{TEHP} differences between different airflow rates. This can be seen from Fig. 6, where for the same airflow outlet temperature, i.e. a similar temperature of the airflow through the TEHP system, the COP_{TEHP} values of the TEHP system for different airflow temperatures are almost the same, showing the small effect of reducing the thermal resistance of the hot side heat exchanger by increasing the airflow. Therefore, Fig. 6 analyses the performance of the TEHPs system depending on the reached airflow outlet temperature. In particular, the developed thermoelectric heat pump can heat airflows between 13 and 23 m^3/h from an ambient temperature of 22 °C to temperatures between 44.5 °C and 139.4 °C with COP_{TEHP} values between 2.44 and 1.13.

The performance of the whole TEHP system, COP_{TEHP}, depends on the performance of each thermoelectric block. Fig. 7 presents the main outputs of the six blocks that are arranged on the x-axis in the airflow direction. The first three are OTEHPs, followed by three pyramidal TTEHPs. There are five graphs, one for each of the voltage supplies (4, 6, 8, 10, and 12 V). The airflow rates are colour-coded: green for 13 m^3/h, red for 18 m^3/h, and blue for 23 m^3/h. Bars represent heat generation

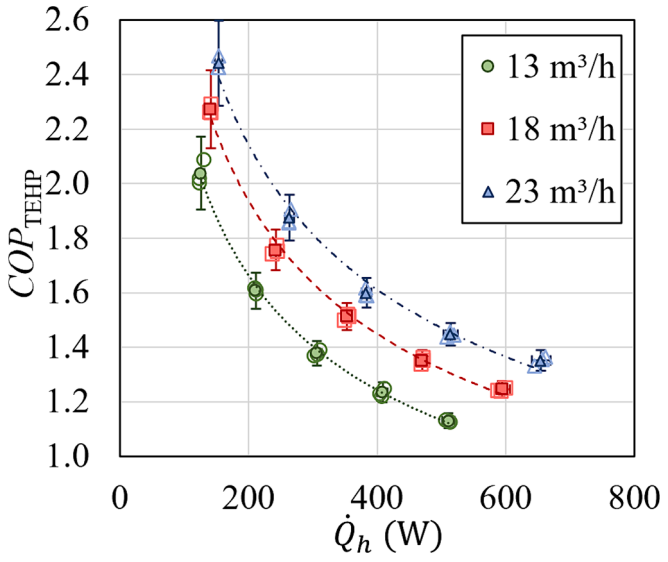

Fig. 5. COP_{TEHP} as function of its heating capacity for different airflow rates.

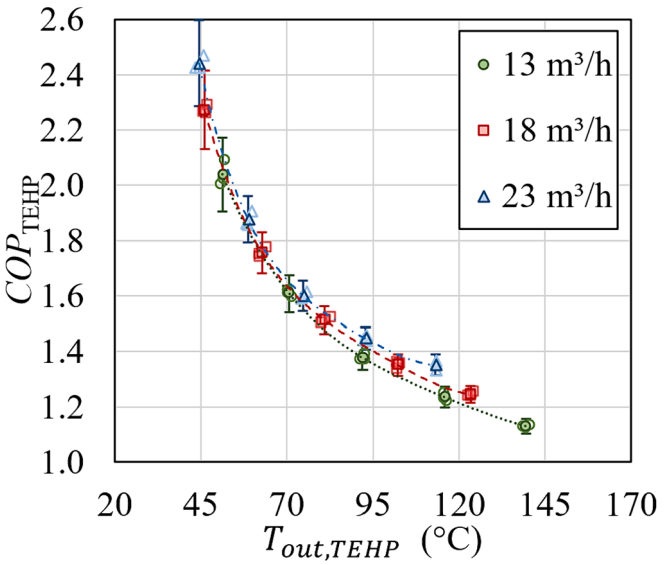

Fig. 6. COP_{TEHP} as function of the airflow outlet temperature ($T_{out,TEHP}$) for different airflow rates.

($\dot{Q}_h$), lines show airflow temperature variation, and data markers represent *COP* values of each thermoelectric heat pump block. In actuality, the correlation between these three key parameters is exhibited, with their reliance on the airflow rate and voltage supply.

Increasing the voltage supply with a constant airflow rate leads to a higher amount of heat being generated by the thermoelectric blocks. This is particularly evident in the y-axis scales, whereby a voltage supply of 4 V results in heat generation ranging from approximately 10 to 45 W, whereas a voltage supply of 12 V yields heat generation between 50 and 200 W. Consequently, when a higher voltage supply is provided, the airflow attains higher temperatures. Additionally, it is worth noting that TTEHPs possess a greater heating capacity than OTHEPs. While OTEHP blocks generate 10–80 W of heat, TTEHPs blocks almost double the heat output, reaching $\dot{Q}_h$ values from 20 to 200 W. In addition, a great temperature tendency change is noticed between the three OTEHP blocks and the following TTEHP blocks in all studied airflow rates.

At the same time, for the same voltage supply when increasing the airflow rates, the heating capacity of all blocks increases. This is because increasing airflow rate results in a decrease in the attained temperature within the airflow. When the airflow rate increases, there is a corresponding increase in the mass airflow. Consequently, a higher amount of heat is required to achieve the same temperature lift in the airflow, as stated in the Eq. (3). The thermoelectric pump blocks operate between lower temperature differences at higher airflow rates, leading to higher *COP* values and subsequently generating more heat for the same voltage supplies.

In relation to the *COP* values of both TEHP configurations, there is a decrease as the airflow temperature increases. As the airflow temperature rises, the temperature difference between sources also increases. The temperature difference between the sources on each block is the difference between the airflow temperature and the ambient temperature, which remains constant. Whereas the temperature of the airflow depends upon both the inlet temperature and the dissipated heat of each thermoelectric block. Thus, the *COP* of either the first three OTEHP or the last three TTEHPs decreases as the airflow temperature increases, as shown in Fig. 7. However, a notorious difference between the performance of the OTEHPs and TTEHPs is shown in all charts. Considering that TTEHP blocks function at higher temperature differentials due to the preheating of airflow by previous OTEHP blocks, the two-stage configuration produces significantly more heat than the one-stage configuration. Furthermore, at voltage supplies higher than 8 V, the

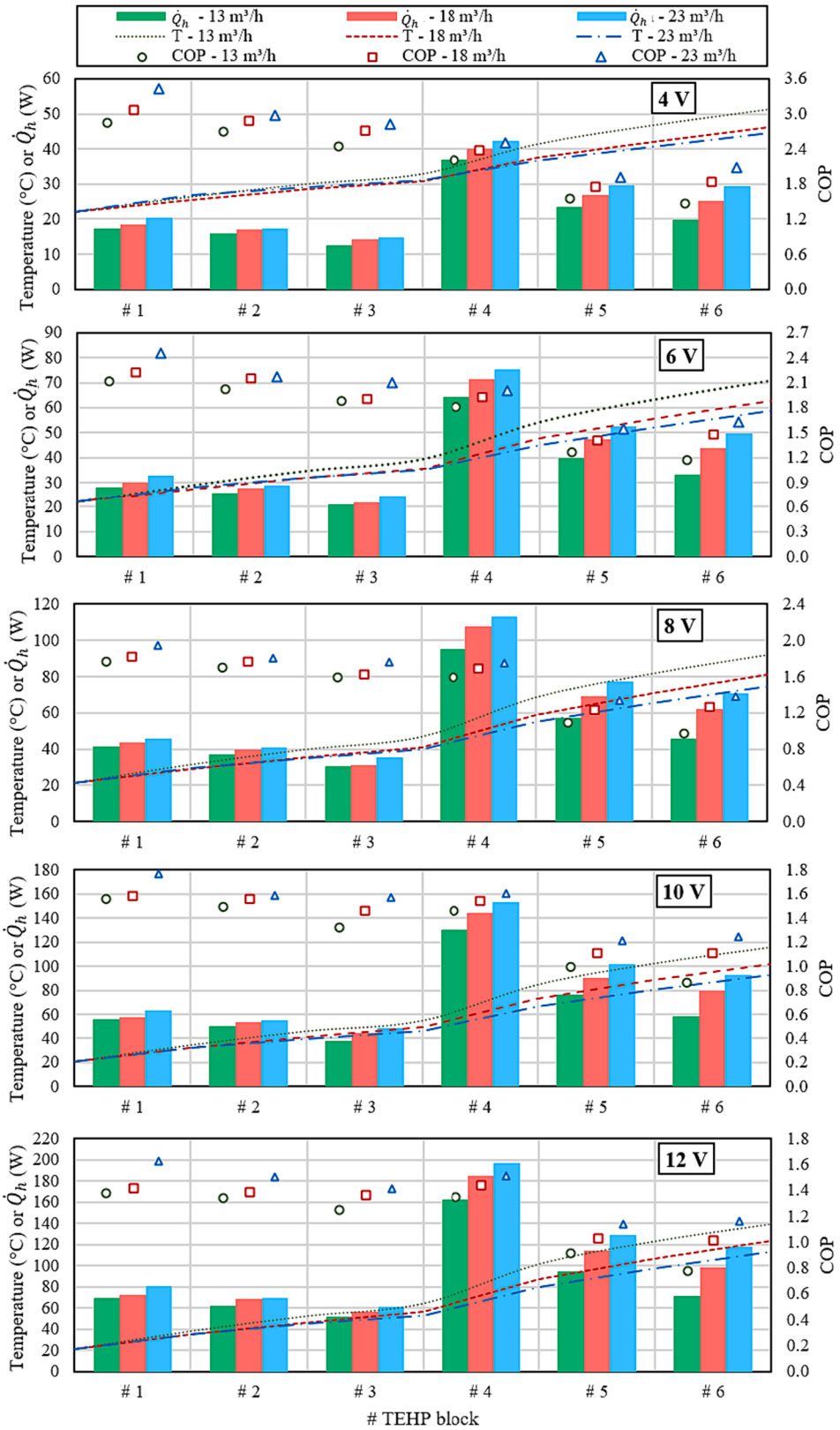

Fig. 7. COP, $\dot{Q}_h$ and airflow temperature variation of TEHP blocks through the duct for different voltage supply.

thermoelectric block number four, featuring a two-stage configuration, not only exhibits similar *COP* values to the third thermoelectric block (which adopts a one-stage configuration), but also effectively doubles the amount of generated heat when operating at higher temperature differences.

In addition, the 10 and 12 V graphs in Fig. 7 show how the last thermoelectric blocks do not work properly, obtaining *COP* values lower than one. This phenomenon arises as a result of the elevated temperature of the airflow entering the TTEHP blocks. As a result, the temperature discrepancy between the sources is elevated, leading to an augmented

natural heat transfer from the hot source to the cold source, because of the Fourier effect. Within those TTEHPs, the natural heat transfer exceeds the heat pumped from the cold source to the hot source through the Peltier effect. Therefore, under those operational conditions, it would be necessary to utilise a three-stage thermoelectric heat pump.

4. Experimental analysis of the influence of the TEHP on the TES system

In the forthcoming section, an analysis is conducted on the performance of the hybridised PtH process, encompassing the TEHP system and the electric resistance. Fig. 8 presents the generated heat by each technology for the different forty five scenarios defined in Table 2. The heat generated by the TEHP system is contingent upon the voltage supply and the COP_{TEHP}, which is influenced by the operating temperatures and airflow rate. It is demonstrated that an increase in voltage supply leads to a corresponding increase in heat generated by the TEHP. In addition, an elevated airflow rate has the simultaneous effect of reducing the temperature difference between sources and diminishing the thermal resistance of the hot heat exchanger. The result is a positive effect on the COP_{TEHP}, resulting in increased heat generation as the airflow rates rise while maintaining the same voltage supply. As an example, when the voltage supply is 6 V, the generated heat at a rate of 13 m^3/h amounts to approximately 211.7 W, resulting in a COP_{TEHP} of 1.61. When the voltage supply is increased by 10 V, the heat generated rises to 408.5 W, resulting in a COP_{TEHP} of 1.23. By increasing the airflow to 23 m^3/h, enhanced performance is attained, resulting in generated heat of 265.7 W and 514.1 W, accompanied by COP_{TEHP} values of 1.88 and 1.45 for voltage supplies of 6 V and 10 V, respectively.

In each scenario, the TEHP system raises the airflow to a particular temperature. Nevertheless, in the majority of cases, this temperature tends to be lower than the value indicated in Table 2. Hence, the electrical resistance is utilised to provide the remaining essential heat, with a COP_{R_e} of one. Fig. 8 clearly demonstrates that the total heat required in each scenario is contingent upon the TES inlet temperature and the airflow rate being utilised. In actuality, the higher they are, the greater the heat required.

The total coefficient of performance of the power-to-heat energy conversion is determined by the performance of the thermoelectric system and electric resistance, as well as the amount of heat generated by each technology, as outlined in Eq. (6). In particular, in Fig. 9 the COP_{PtH} values of the TEHP system under various voltage supplies are depicted in the forty-five scenarios. There is shown that for a particular airflow rate exists an optimal voltage supply to the TEHP system. For an airflow rate of 13 m^3/h the optimal voltage is 8 V, achieving COP_{PtH} values between 1.24 and 1.12, for 18 m^3/h the optimal voltage is 10 V, achieving COP_{PtH} values between 1.26 and 1.13, and for 23 m^3/h the optimal voltage is 12 V, achieving COP_{PtH} values between 1.30 and 1.15 for the storage temperatures ranging between 120 °C and 200 °C, respectively. Specifically, as the airflow rate increases, the optimal voltage value also increases. Furthermore, it is noteworthy that the optimal voltage supply for power-to-heat conversion may not necessarily be the same as the one that yields the highest COP_{TEHP} or the greatest amount of generated heat with the TEHP system (Fig. 8). Specifically, it considers the percentage of heat generated by the TEHP system and its COP_{TEHP}, as the greater the heat generated by the electric heaters, the closer the COP_{PtH} will be to unity.

5. Experimental analysis of the TES charging process

In the experimental campaign, the TES charging process is considered to be complete when the TES outlet airflow temperature is 40 °C lower than the TES inlet airflow temperature. The energy absorption of steel balls is caused by the natural heat flow, which is a result of the temperature difference between the incoming air and the stored material. As time progresses, the stored material undergoes a rise in temperature, thereby effectively storing energy in the form of heat. As the temperature of the stainless steel balls increases, the heat transferred from the air decreases because of the reduced temperature difference. Therefore, the temperature of the air released from the thermal storage will gradually rise, resulting in an effective charging of the thermal energy storage system.

Fig. 10 shows the different inlet and outlet temperatures over time for the different air flow rates and storage temperatures studied. To obtain these curves, the optimum voltage supply to the TEHP system is chosen: 8, 10 and 12 V at 13, 18 and 23 m^3/h, respectively. As expected, $T_{in,TES}$ remains constant while $T_{out,TES}$ increases with time. The higher the storage temperature, the longer it takes for the TES charging process to be completed. However, it can be observed that at higher $T_{in,TES}$, the heat transfer from the air to the storage mediums is enhanced at the beginning of the test, primarily due to a more pronounced temperature difference between the air and storage material. Additionally, the higher the airflow rate, the shorter the charging time for the TES. This phenomenon occurs due to the enhancement of convective heat transfer between the airflow and the stainless steel balls at higher airflow rates. In particular, the minimum time is reached at 23 m^3/h, where 1.5, 2.2 and 2.4 h are required to complete the charging process for 120, 160 and 200 °C respectively. Furthermore, the use of the highest airflow rate gives the best PtH performance, with COP_{PtH} values of 1.3, 1.21 and 1.15 respectively. In this case, the heating energy required to complete the load is calculated by multiplying the heat generated by the TEHP system and the electrical resistance by the duration of the test. In fact, 1.2, 2.5 and 4.1 kWh_t of thermal energy are generated to complete the load of the TES at 120, 160 and 200 °C by consuming 1.0, 2.1 and 3.1 kWh_e of electrical energy respectively.

6. Case of study

This final section outlines the potential of combining the developed prototype, which incorporates a TEHP system, and electric resistance technology for heat storage applications, with a heat-to-power system. The focus of this analysis lies in the utilisation of a power-to-heat-to-

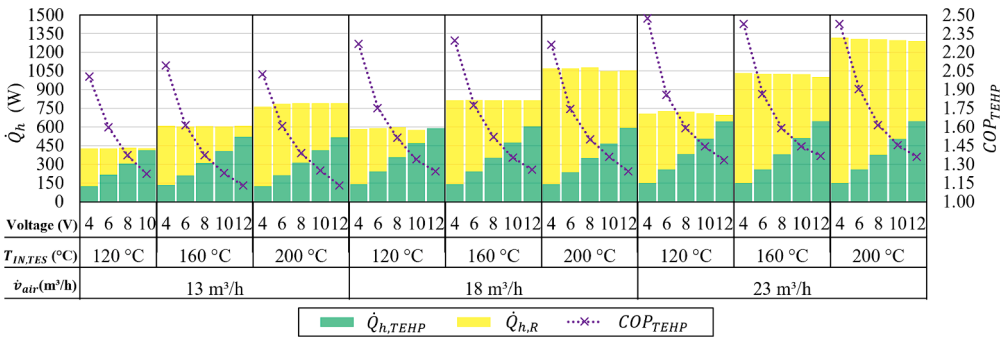

Fig. 8. Qh and COP values for TEHP and the coupling of TEHP with electric resistances.

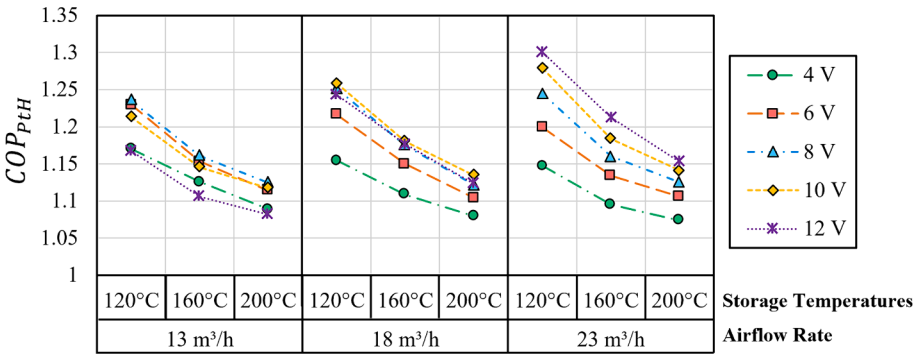

Fig. 9. COP_{PtH} in each scenario for different voltage supply.

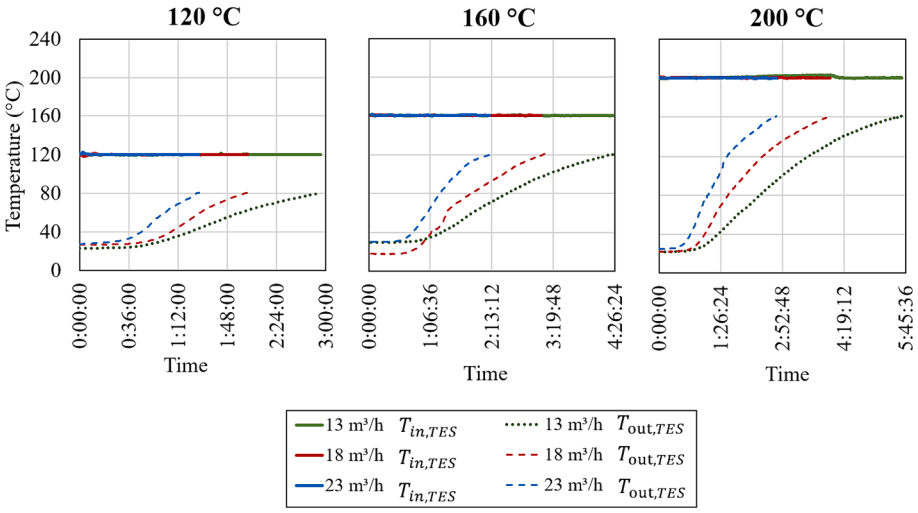

Fig. 10. TES inlet and outlet temperature for the optimum TEHP system voltage supplies.

power (PtHtP) system, which enables the storage of excess renewable energy and its subsequent conversion into electrical energy as the need arises.

The conversion of energy from power to heat relies on the experimental data gathered in this manuscript. Specifically, the experimental data collected at an airflow rate of 23 m^3/h and a TEHP system voltage of 12 V is utilised. The heat-to-power process incorporates the experimental outcomes of the ORC investigation conducted by Qiu and Entchev [49]. A combined heat and power installation has been constructed for residential heating and power generation. This installation employs an ORC cycle, utilising R1233zd(E) refrigerant, along with an evaporator, preheater, scroll expander, generator, condenser, low temperature recuperator, and gas-fired boiler as a heat source. The range of ORC efficiencies observed was between 6.6 % and 10.3 %, which were attained by manipulating the expander inlet temperatures within the range of 125 °C to 165 °C, while keeping a constant pressure ratio of 3.65. The combination of power and heat generation resulted in a CHP efficiency of 89.2 %, achieved at an expander inlet temperature of 135 °C and a pressure ratio of 3.65.

In the context of this study, the TES will serve as the heat source for the ORC. The analysis of the combination of both technologies takes into account the ideal temperature for the TES, assuming that the expander inlet temperature of the ORC and the storage temperature are equal. The efficiency of the PtHtP system (η_{PtHtP}) is evaluated by Eq.9. It relates the expander shaft power (P_{shaft}), divided by the consumption of the PtH process ($\dot{W}_{e,TEHP} + \dot{W}_{e,R}$).

$$\eta_{PtHtP} = \frac{P_{shaft}}{\dot{W}_{e,TEHP} + \dot{W}_{e,R}} \tag{9}$$

Eq.10 presents the efficiency of the PtHtP process defined by the COP_{PtH} of the PtH process and the efficiency of the ORC (η_{ORC}).

$$\eta_{PtHtP} = COP_{PtH} \cdot \eta_{ORC} \tag{10}$$

The installation of the TEHP system outperforms the η_{PtHtP} in a 15–30 % compared to using conventional electrical resistors to heat up the TES up to 165–125 °C. Specifically, η_{PtHtP} values ranged between 8.5 and 12.4 % are achieved. In addition, in the study of Qiu and Entchev [49], the application of the studied PtH system in a CHP system is evaluated, being a power-to-heat-to-combined heat and power (PtHtCHP) system. Its efficiency ($\eta_{PtHtCHP}$) is assessed by Eq. (11), which relates the generated useful power from the expander and the useful heat (P_h) with the total consumed electric energy.

$$\eta_{PtHtCHP} = \frac{P_{shaft} + P_h}{\dot{W}_{e,TEHP} + \dot{W}_{e,R}} \tag{11}$$

As function of the COP_{PtH} and the CHP efficiency (η_{CHP}), Eq.12 is obtained.

$$\eta_{PtHtCHP} = COP_{PtH} \cdot \eta_{CHP} \tag{12}$$

The implementation of a TEHP to feed the ORC system supposes an increase from 89.2 % to 112.6 % in the $\eta_{PtHtCHP}$ at an expander inlet temperature of 135 °C, improving in a 26 % the global efficiency when the TEHP system is included. Values greater than 100 % are possible to be obtained in a PtHtCHP system because the COP_{PTH} is greater than one.

In this case, the combination of the TEHP system and the electric resistance obtains a COP_{PTH} of 1.26. Thus, the potential of thermoelectric technology to charge combined heat and power generation processes has been demonstrated, obtaining heat and electric power at the same time. In fact, the PtHtCHP process obtains more useful power than the consumed electric power.

6.1. Comparison

To highlight the favourable results attained through the utilisation of thermoelectric technology, it is pertinent to make a comparative analysis with other analogous investigations. Indeed, there has been a growing interest in pumped thermal energy storage systems utilising vapor compression heat pumps. The performance of power-to-heat energy conversion directly affects the effectiveness of PtHtP and PtHtCHP systems (Eq. (10) and (12). Therefore, the performance of the developed TEHP system, supplemented by electrical resistance, has to be compared with existing VCHP systems, which are given in Table 3.

There has been demonstrate that the developed TEHP system with electric resistances obtains COP_{PTH} values of 1.30 and 1.15 for the storage temperatures ranging between 120 °C and 200 °C, respectively. Consequently, the thermoelectric system that has been developed attains COP_{PtH} values that are similar to those of the single-stage VCHPs. Nonetheless, when contrasting with complex VCHP configurations, the developed system yields a lower COP_{PtH}. Hence, it is imperative to conduct more research to explore diverse setups of the TEHP system. Moreover, thermoelectric technology offers the advantage of scalability and modularity, requiring no refrigerants or moving components. Additionally, it is noteworthy that most studies employ higher source temperatures, leading to improved performance due to the decrease in temperature difference between sources. Thus, a comprehensive study of the developed TEHP system at different source temperatures is required.

7. Conclusion

This manuscript has been focused on the analysis of the developed high temperature thermoelectric heat pump system. The analysis focuses on assessing the coefficient of performance and heating capacity by varying the voltage supply and the airflow rate, in order to achieve higher temperatures in an airflow. The developed TEHP system consists of a series of three one-stage and three two-stage TEHP blocks arranged in the direction of airflow. The following main findings emerge from the present experimental study:

- The performance of both one-stage and two-stage thermoelectric blocks deteriorates with increasing airflow temperature, as they are required to function at greater temperature differentials. The increase in voltage supply leads to a corresponding rise in the generated heat. For the same airflow rate, the airflow temperature will be higher at higher supply voltages, resulting in a reduction in performance. In relation with this, greater airflows lead to elevated COP_{TEHP} due to the attainment of lower temperatures with the same generated heat. With the highest studied airflow rate (23 m^3/h), 655.5 W of heat can be generated with a COP_{TEHP} of 1.35, elevating the airflow temperature from the ambient temperature to 113.1 °C.
- The capability of achieving high temperatures with thermoelectric technology is being showcased for the first time, owing to its modular nature and the ability to employ multiple-stage configurations, thereby expanding the scope of its potential applications.
- There is demonstrate that the two-stage configuration exhibits over twice the heating capacity respect one-stage configuration, despite consistently operating at higher temperatures. Moreover, it is shown how at high temperatures it is only possible to work with configurations with more than one stage, which provides a better performance.
- The integration of the developed TEHP system into the charging process of a thermal energy storage system based on electrical resistances increases the energy conversion efficiency by 15 % and 30 % for energy storage temperatures between 120 and 200 °C. This improvement depends mainly on the performance of the TEHP system and the amount of heat generated by the TEHP system and the electrical resistance. The TEHP system also offers seamless integration with other heating systems.

The great potential of thermoelectric technology to efficiently convert surplus renewables into heat has been demonstrated. The advantages of thermoelectricity, such as its scalability, modularity, and lack of refrigerants, make it a promising technology for heating. The present study is the first experimental study where a thermoelectric heat pump system including two-stage configuration is used for achieving high temperatures in a real application. However, further studies are necessary to explore its full potential. Specifically, further research is needed to understand its behaviour under varying cold source temperatures, given the potential focus on waste heat recovery for industrial and buildings applications. Furthermore, there is the opportunity to explore the utilisation of different heating fluids, including the integration of phase change materials for the purpose of energy storage.

CRediT authorship contribution statement

I. Erro: Writing – review & editing, Writing – original draft, Data curation, Conceptualization. **P. Aranguren:** Writing – review & editing, Supervision, Project administration, Funding acquisition. **F.J. Sorbet:** Resources, Funding acquisition. **I. Bonilla-Campos:** Visualization, Investigation. **D. Astrain:** Supervision, Project administration, Funding acquisition.

Declaration of competing interest

The authors declare the following financial interests/personal relationships which may be considered as potential competing interests:

Table 3
Performance of different VCHPs (Based on [44]).

Technology	Source Fluid	Working Fluid	Heated Fluid	Source Temperature [°C]	Storage temperature [°C]	COP_{PtH} [-]
Single-stage VCHP [33]	Water	R1234ze(Z)	Water	40	100	**1.4**
				50	120	**1.25**
Single-stage VCHP [50]	Water	R1336mzz(Z)	Water	60	130	**1.4**
Single-stage VCHP [50]	Water	R1224yd(Z)	Water	70	140	**1.5**
Single-stage VCHP with IHX [33]	Water	R1234ze(Z)	Water	40	120	**1.37**
Two-stage VCHP [33]	Water	R1234ze(Z)	Water	40	150	**1.53**
Two-stage VCHP with a FTVI [35]	Air	R-744	Water	7	72	**1.98**
Three-stage VCHP [34]	Air	R-718/ R-600/ R-600	Air	50	210	**1.92**
Reversed Brayton Cycle [51]	Air	Air	Water	5	65	**1.9**
Reversed Brayton Cycle [34]	Air	R-744	Air	50	210	**1.61**

Irantzu Erro reports financial support was provided by Navarra Government. Patricia Aranguren reports financial support was provided by Navarra Government.

Data availability

The data that has been used is confidential.

Acknowledgments

The authors would like to acknowledge the support of the Government of Navarre, as part of the "Grants to SINAI agents for the realisation of collaborative R&D projects" under the PC066-067-068 FlexORC-Storage project. Open access funding provided by Universidad Pública de Navarra.

References

[1] Renewable Energy Agency I. WORLD ENERGY TRANSITIONS OUTLOOK 1.5° C PATHWAY. 2021.
[2] THE 17 GOALS | Sustainable Development. https://sdgs.un.org/goals (accessed January 24, 2024).
[3] Statistics | Eurostat. https://ec.europa.eu/eurostat/databrowser/view/nrg_ind_ren/default/table?lang=en (accessed June 14, 2023).
[4] Share of energy consumption from renewable sources in Europe. https://www.eea.europa.eu/en/analysis/indicators/share-of-energy-consumption-from?activeAccordion=ecdb3bcf-bbe9-4978-b5cf-0b136399d9f8 (accessed January 9, 2024).
[5] I. Bonilla-Campos, F.J. Sorbet, D. Astrain, Radical change in the Spanish grid: Renewable energy generation profile and electric energy excess, Sustain. Energy Grids Netw. 32 (2022), https://doi.org/10.1016/J.SEGAN.2022.100941.
[6] G. Sadeghi, Energy storage on demand: Thermal energy storage development, materials, design, and integration challenges, Energy Storage Mater. 46 (2022) 192–222, https://doi.org/10.1016/J.ENSM.2022.01.017.
[7] B. Eppinger, L. Zigan, J. Karl, S. Will, Pumped thermal energy storage with heat pump-ORC-systems: Comparison of latent and sensible thermal storages for various fluids, Appl. Energy 280 (2020), https://doi.org/10.1016/j.apenergy.2020.115940.
[8] E. Guelpa, V. Verda, Thermal energy storage in district heating and cooling systems: A review, Appl. Energy 252 (2019) 113474, https://doi.org/10.1016/J.APENERGY.2019.113474.
[9] N.T. Bin, M. Siddiqui, M. Khalid, M. Asif, Distributed energy systems: A review of classification, technologies, applications, and policies, Energy Strategy Rev. 48 (2023), https://doi.org/10.1016/j.esr.2023.101096.
[10] O.A. Rehman, V. Palomba, A. Frazzica, L.F. Cabeza, Enabling technologies for sector coupling: A review on the role of heat pumps and thermal energy storage, Energies (Basel) 14 (2021), https://doi.org/10.3390/en14248195.
[11] H.M. Ali, T.ur. Rehman, M. Arıcı, Z. Said, B. Duraković, H.I. Mohammed, et al. Advances in thermal energy storage: Fundamentals and applications. Prog. Energy Combust. Sci. 2024;100. doi:10.1016/j.pecs.2023.101109.
[12] M. Tawalbeh, H.A. Khan, A. Al-Othman, F. Almomani, S. Ajith, A comprehensive review on the recent advances in materials for thermal energy storage applications, Int. J. Thermofluids 18 (2023) 100326, https://doi.org/10.1016/J.IJFT.2023.100326.
[13] S.C. Costa, M. Kenisarin, A review of metallic materials for latent heat thermal energy storage: Thermophysical properties, applications, and challenges, Renew. Sustain. Energy Rev. 154 (2022), https://doi.org/10.1016/j.rser.2021.111812.
[14] H. Agalit, N. Zari, M. Maaroufi, Thermophysical and chemical characterization of induction furnace slags for high temperature thermal energy storage in solar tower plants, Sol. Energy Mater. Sol. Cells 172 (2017) 168–176, https://doi.org/10.1016/j.solmat.2017.07.035.
[15] F. Afsharpanah, S.S. Mousavi Ajarostaghi, M. Arıcı, Parametric study of phase change time reduction in a shell-and-tube ice storage system with anchor-type fin design, Int. Commun. Heat Mass Transf. 137 (2022), https://doi.org/10.1016/j.icheatmasstransfer.2022.106281.
[16] S. Soprani, F. Marongiu, L. Christensen, O. Alm, K.D. Petersen, T. Ulrich, et al., Design and testing of a horizontal rock bed for high temperature thermal energy storage, Appl. Energy 251 (2019), https://doi.org/10.1016/j.apenergy.2019.113345.
[17] K. Knobloch, Y. Muhammad, M.S. Costa, F.M. Moscoso, C. Bahl, O. Alm, et al., A partially underground rock bed thermal energy storage with a novel air flow configuration, Appl. Energy 315 (2022), https://doi.org/10.1016/j.apenergy.2022.118931.
[18] L. Yang, H. Xu, F. Cola, B. Akhmetov, A. Gil, L.F. Cabeza, et al., Shell-and-tube latent heat thermal energy storage design methodology with material selection, storage performance evaluation, and cost minimization, Appl. Sci. (Switzerland) 11 (2021), https://doi.org/10.3390/app11094180.
[19] R.D. Selvakumar, J. Wu, I. Afgan, Y. Ding, A.K. Alkaabi, Melting performance enhancement in a thermal energy storage unit using active vortex generation by electric field, J. Energy Storage 67 (2023), https://doi.org/10.1016/j.est.2023.107593.
[20] H. Lin, C. Zhai, F. Li, Y. Sui, W. Wu, Multidimensional assessment of commercial-scale power-to-heat batteries for high energy flexibility, Energy Convers. Manag. 294 (2023), https://doi.org/10.1016/j.enconman.2023.117606.
[21] D. Laing, C. Bahl, T. Bauer, D. Lehmann, W.D. Steinmann, Thermal energy storage for direct steam generation, Sol. Energy 85 (2011) 627–633, https://doi.org/10.1016/J.SOLENER.2010.08.015.
[22] J. Van Nieuwenhuyse, M. De Paepe, S. Lecompte, T. Srinivas, I.K. Smith, Rankine cycle and variants, Power Gen. Technol. Low-Temp. Distrib. Heat, Elsevier (2023) 49–161, https://doi.org/10.1016/B978-0-12-818022-8.00001-6.
[23] M.A. Qyyum, A. Khan, S. Ali, M.S. Khurram, N. Mao, A. Naquash, et al., Assessment of working fluids, thermal resources and cooling utilities for organic rankine cycles: State-of-the-art comparison, challenges, commercial status, and future prospects, Energy Convers. Manag. 252 (2022) 115055, https://doi.org/10.1016/J.ENCONMAN.2021.115055.
[24] D. Fiaschi, G. Manfrida, E. Rogai, L. Talluri, Exergoeconomic analysis and comparison between ORC and Kalina cycles to exploit low and medium-high temperature heat from two different geothermal sites, Energy Convers. Manag. 154 (2017) 503–516, https://doi.org/10.1016/j.enconman.2017.11.034.
[25] K. Rahbar, S. Mahmoud, R.K. Al-Dadah, N. Moazami, S.A. Mirhadizadeh, Review of organic Rankine cycle for small-scale applications, Energy Convers. Manag. 134 (2017) 135–155, https://doi.org/10.1016/J.ENCONMAN.2016.12.023.
[26] I. Cruz, M.T. Johansson, J. Wren, Assessment of the potential for small-scale CHP production using Organic Rankine Cycle (ORC) systems in different geographical contexts: GHG emissions impact and economic feasibility, Energy Rep. 8 (2022) 7680–7690, https://doi.org/10.1016/j.egyr.2022.06.006.
[27] J.R. Eggers, M. von der Heyde, S.H. Thaele, H. Niemeyer, T. Borowitz, Design and performance of a long duration electric thermal energy storage demonstration plant at megawatt-scale, J. Energy Storage 55 (2022), https://doi.org/10.1016/j.est.2022.105780.
[28] J. Iñigo-Labairu, J. Dersch, L. Schomaker, Integration of CSP and PV power plants: Investigations about synergies by close coupling, Energies (Basel) 15 (2022), https://doi.org/10.3390/en15197103.
[29] W. Hu, R. Sun, K. Zhang, M. Liu, J. Yan, Thermoeconomic analysis and multiple parameter optimization of a combined heat and power plant based on molten salt heat storage, J. Energy Storage 72 (2023), https://doi.org/10.1016/j.est.2023.108698.
[30] I. Dincer, 1.7 energy and exergy efficiencies, Compr. Energy Syst. 1–5 (2018) 265–339, https://doi.org/10.1016/B978-0-12-809597-3.00123-1.
[31] K. Hamid, U. Sajjad, M. Ulrich Ahrens, S. Ren, P. Ganesan, I. Tolstorebrov, et al., Potential evaluation of integrated high temperature heat pumps: A review of recent advances, Appl. Therm. Eng. (2023) 230, https://doi.org/10.1016/j.applthermaleng.2023.120720.
[32] C. Arpagaus, F. Bless, M. Uhlmann, J. Schiffmann, S.S. Bertsch, High temperature heat pumps: Market overview, state of the art, research status, refrigerants, and application potentials, Energy 152 (2018) 985–1010, https://doi.org/10.1016/J.ENERGY.2018.03.166.
[33] G. Kosmadakis, C. Arpagaus, P. Neofytou, S. Bertsch, Techno-economic analysis of high-temperature heat pumps with low-global warming potential refrigerants for upgrading waste heat up to 150 °C, Energy Convers. Manag. (2020) 226, https://doi.org/10.1016/j.enconman.2020.113488.
[34] B. Zühlsdorf, F. Bühler, M. Bantle, B. Elmegaard, Analysis of technologies and potentials for heat pump-based process heat supply above 150 °C, Energy Convers. Manage. X (2019) 2, https://doi.org/10.1016/j.ecmx.2019.100011.
[35] L.Z. Bin, L. Ma, Z. Qian, Y.L. He, Experimental study on performance of the trans-critical CO2 heat pump with flash tank vapor injection at variable revolution ratio conditions, J. Clean. Prod. 412 (2023), https://doi.org/10.1016/j.jclepro.2023.137405.
[36] D. Rowe, Raton London New York B. Thermoelectrics Handbook. CRC Press; 2018. doi:10.1201/9781420038903.
[37] S. Diaz de Garayo, A. Martínez, P. Aranguren, D. Astrain, Prototype of an air to air thermoelectric heat pump integrated with a double flux mechanical ventilation system for passive houses, Appl. Therm. Eng. 190 (2021) 116801, https://doi.org/10.1016/j.applthermaleng.2021.116801.
[38] B. Hou, Y. Zheng, L. Xing, Q. Song, Performance of a thermoelectric heat pump with recirculation and regenerative heat recovery, Appl. Therm. Eng. (2023) 223, https://doi.org/10.1016/j.applthermaleng.2023.120042.
[39] H. Nami, A. Nemati, M. Yari, F. Ranjbar, A comprehensive thermodynamic and exergoeconomic comparison between single- and two-stage thermoelectric cooler and heater, Appl. Therm. Eng. 124 (2017) 756–766, https://doi.org/10.1016/j.applthermaleng.2017.06.100.
[40] L. Chen, J. Li, F. Sun, C. Wu, Performance optimization for a two-stage thermoelectric heat-pump with internal and external irreversibilities, Appl. Energy 85 (2008) 641–649, https://doi.org/10.1016/J.APENERGY.2007.10.005.
[41] R. Arora, Multiobjective optimization and analytical comparison of single- and 2-stage (series/parallel) thermoelectric heat pumps, Int. J. Energy Res. 42 (2018) 1760–1778, https://doi.org/10.1002/er.3988.
[42] L.G. Chen, F.K. Meng, Y.L. Ge, H.J. Feng, S.J. Xia, Performance optimization of a class of combined thermoelectric heating devices, Sci. China Technol. Sci. 63 (2020) 2640–2648, https://doi.org/10.1007/s11431-019-1518-x.
[43] I. Erro, P. Aranguren, P. Alegría, A. Rodriguez, D. Astrain, Advanced phase-change intermediate heat exchanger development for multistage thermoelectric heat pumps, Therm. Sci. Eng. Prog. 47 (2024) 102298, https://doi.org/10.1016/j.tsep.2023.102298.
[44] I. Erro, P. Aranguren, I. Alzuguren, D. Chavarren, D. Astrain, Experimental analysis of one and two-stage thermoelectric heat pumps to enhance the performance of a

thermal energy storage, Energy (2023) 285, https://doi.org/10.1016/j.energy.2023.129447.
[45] RC12-6-01LS Marlow Industries, Inc. | Fans, Thermal Management | DigiKey n.d. https://www.digikey.es/en/products/detail/marlow-industries-inc/RC12-6-01LS/6159103?s=N4IgTCBcDaIEoGECMYC0A2VAGJAZAyiALoC%2BQA (accessed January 28, 2022).
[46] Technical Data Sheet for TG12-6 Single-Stage Thermoelectric Generator NOMINAL PERFORMANCE IN NITROGEN. n.d.
[47] Moran MJ, Shapiro HN, Bailey MB. Fundamentals of Engineering Thermodynamics 9th Edition. n.d.
[48] Hugh W. Coleman, Steele WG. Experimentation, validation, and uncertainty analysis for engineers 3rd ed. 2019.
[49] K. Qiu, E. Entchev, A micro-CHP system with organic Rankine cycle using R1223zd (E) and n-pentane as working fluids, Energy 239 (2022) 121826, https://doi.org/10.1016/J.ENERGY.2021.121826.
[50] Arpagaus C, Bertsch SS, Buchs N. Experimental results of HFO/HCFO refrigerants in a laboratory scale HTHP with up to 150 °C supply temperature. 2019.
[51] C.L. Zhang, H. Yuan, An important feature of air heat pump cycle: Heating capacity in line with heating load, Energy 72 (2014) 405–413, https://doi.org/10.1016/j.energy.2014.05.055.